Supplement of The Cryosphere, 15, 1435–1451, 2021
https://doi.org/10.5194/tc-15-1435-2021-supplement

The Cryosphere Open Access EGU

Supplement of

Basal traction mainly dictated by hard-bed physics over grounded regions of Greenland

Nathan Maier et al.

Correspondence to: Nathan Maier (ntmaier@gmail.com)

Table of Contents

Supplementary Analysis

1. Estimating traction variability due to data error and uncertainty

Data errors and uncertainty arise from the methodologies used to measure ice velocities (Joughin et al., 2018) and estimate ice thickness (Morlighem et al., 2017). The velocity error and uncertainty is a function of the sensor resolution, ice speed, surface slope, and elapsed time between the image pairs used to calculate surface displacements (Joughin et al., 2018). For ice thickness, high error and uncertainty occur in regions where there are few radar measurements to constrain ice thickness (*Figure S7*) (Morlighem et al., 2017). For the grid cells used in the analysis, the average error and uncertainty for each variable is small relative to the magnitude of the value, with magnitudes on the order of 5% and 10% for the velocity and ice thickness respectively averaged over the ice sheet.

We use a Monte Carlo analysis to assess the combined influence of the data error and uncertainty on the variability observed in the velocity – traction relationships. We first calculate the variability (1 σ) in the driving stress (SIA) for each velocity bin for all catchments. Assuming a normally distributed error and uncertainty, we then complete 1000 simulations where the driving stress for each bin is recalculated using randomly resampled data sets given the error and uncertainty for each grid cell. We quantify the approximate variability due data error and uncertainty in the data by taking the standard deviation of the tractions in the velocity bins from the entire ensemble of simulations. This can be directly compared to the observed traction variability in each velocity bin as shown in *Figure S6*. The inverted traction fields of the SSA and FS models are also subject to the same data errors, but the regularization schemes used during the numerical inversion decrease the effect of randomized errors and uncertainty on the traction solutions (Gagliardini et al., 2013). However, we note the traction field for all the inversion methods will still be susceptible to spatially correlated errors which is not specifically quantified here.

We find data error and uncertainty account for 12% of the SIA traction variability averaged across all bins and catchments and therefore cannot account for all the variability observed from the traction relationships in *Figure S6*. However, we also find the proportion of variability due to error and uncertainty varies between bins and catchments. Within each catchment the combined error and uncertainty account for the following percentages of the observed traction variability: 1 – 10%, 2 – 04%, 3 – 14%, 4 – 10%, 5 – 28%, 6 – 07%, 7 – 12%, 8 – 13%. There is generally a higher overall percentage of the variability due to error and uncertainty at the lowest and highest velocities. At low velocities this results from high relative velocity errors due to slow-moving ice (Joughin et al., 2018) and high traction error that result from fewer flight transects that at act as constraints on the mass-conserving bed (Morlighem et al., 2017). For high velocities the high uncertainty mainly results from only having a small set of data points to estimate the variability for each bin.

2. Assessment of n variability

We find it plausible that n, which controls the nonlinearity of both deformation and sliding, could vary systematically in space across Greenland and cause changes in the traction relationships unrelated to the basal properties. Variations n are thought to arise from changes in the dominant deformation mechanism as the deviatoric stress increases in magnitude (Alley, 1992; Cuffey and Paterson, 2010; Montagnat and Duval, 2004). Experimental work has found n ranging from ~1 – 4 and with a transition from $n \approx 2$ to $n \approx 3$ commonly found between 0.05 – 0.1 MPa (Alley, 1992; Montagnat and Duval, 2004). However, in more comprehensive laboratory experiments where deformation reached high total strains as is expected naturally, $n \approx 3$ was found through the entire range of glaciologically relevant stresses (Russell-Head and Budd, 1979). This is consistent with data from most field experiments which indicate that $n \approx 3$ over a wide range of stress conditions (> 0.02 MPa) (Cuffey and Paterson, 2010).

In Greenland n has been estimated from 2.3 – 4.5 using a variety in situ of techniques (Bons et al., 2018; Dahl-Jensen and Gundestrup, 1987; Gillet-Chaulet et al., 2011; Lüthi et al., 2002; Ryser et al., 2014b). This range is large and could reflect real variability in n or conversely uncertainty in the different methodological approaches. There is no coherence in the data that strongly suggests n increases with stress conditions, as the highest values of n were found within the low stress regions where the bed is frozen (Bons et al., 2018; Gillet-Chaulet et al., 2011). However, one of these experiments, which investigated spatially varying velocities and tractions over Greenland's frozen regions, found an apparent change from $n = 2$ to $n = 4$ at ~ 0.04 MPa (Bons et al., 2018). We don't observe obvious knickpoints

that would suggest n changes (*Figure S5*), yet, we do see variability in the n between catchments which spans the range of 2.3 – 4.1. Thus, while we don't have any conclusive evidence to consider it likely, it still remains possible that the n values in the thawed regions have the potential to be higher than in the frozen regions and therefore no increase in nonlinear processes at the base would be required to reach p values of ~ 4. Although even though possible, given the well document presence of hydrologic forcing over hard and till bed boundaries (Andrews et al., 2014, 2018; Bartholomew et al., 2010, 2011, 2012; Cowton et al., 2016; Hoffman et al., 2011; Kulessa et al., 2017; Ryser et al., 2014a; Sole et al., 2013; Stevens et al., 2015), we find presence of cavitation and deforming till a more plausible explanation for the increase in p over n found in our analysis.

Supplementary Figures

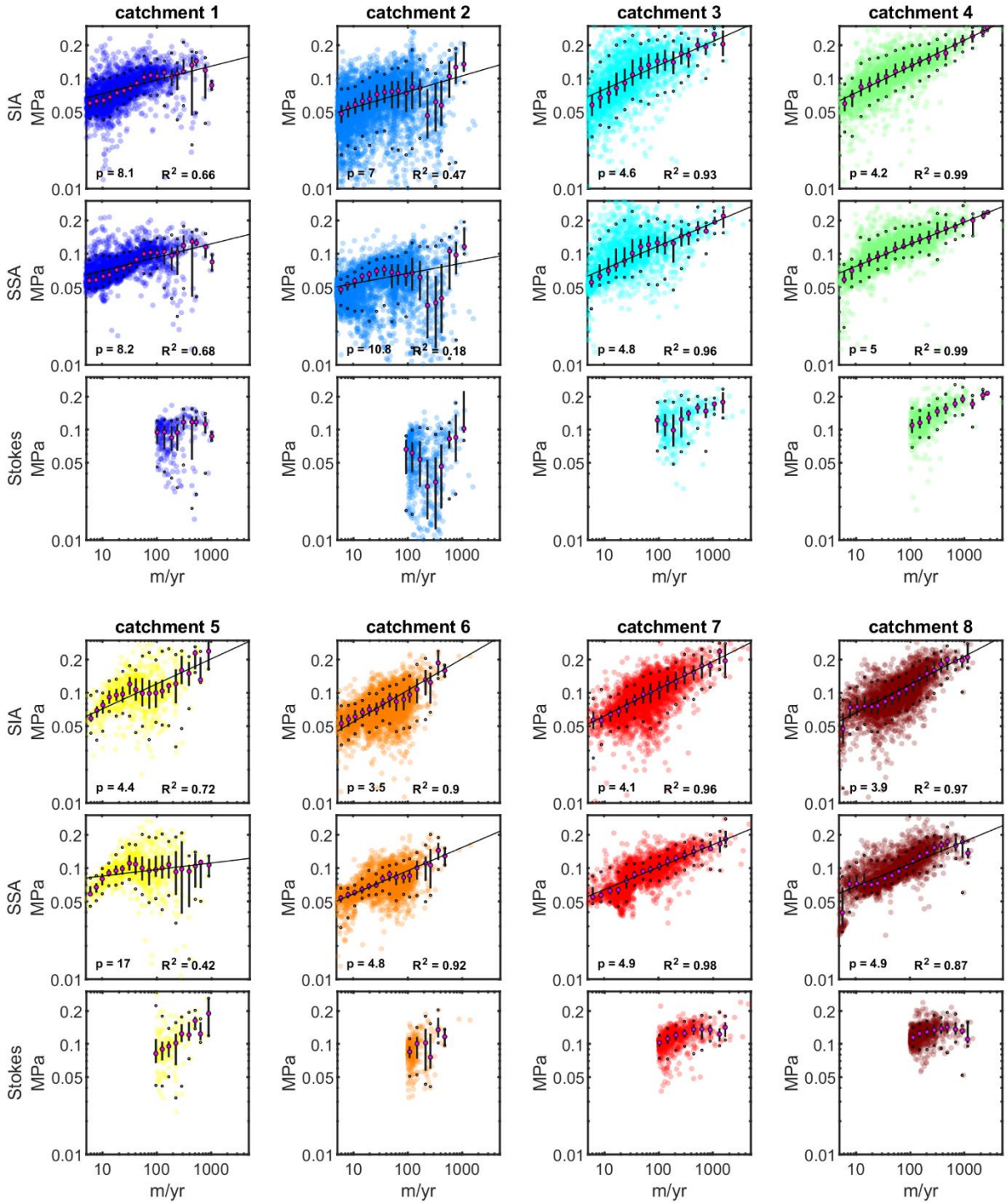

Figure S1 – The velocity – traction relationship for the SIA , SSA, and Full Stokes inversions (6 km) including the uncertain regions of the basal thermal state mask. Transparency is an indicator of data density, where opaque areas indicate four or more grid cells occupy the same marker area on the plot. Magenta markers show the median traction values for 20 logarithimically spaced velocity bins, the vertical bars show the interquartile range, and the black dots

indicate the middle 90th percentile of the data. Black line shows a power law model fit to the binned data. No models were fit to the stokes relationships due to the velocity range (> 100 m/yr) which is limited in our analysis.

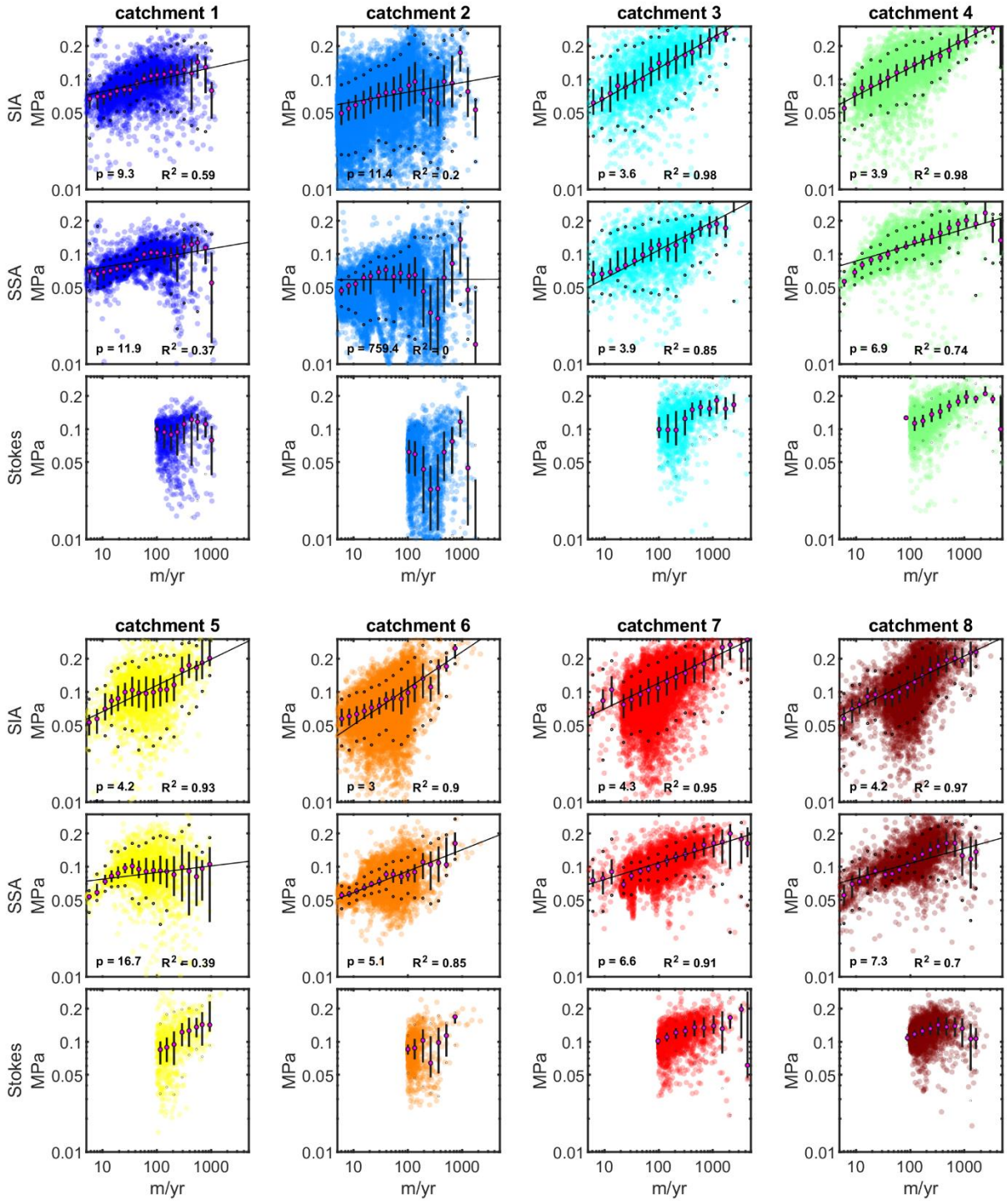

Figure S2 – The velocity – traction relationship for the SIA , SSA, and Full Stokes inversions using 3 km grid cells. Transparency is an indicator of data density, where opaque areas indicate four or more grid cells occupy the same marker area on the plot. Magenta markers show the median traction values for 20 logarithimically spaced velocity bins, the vertical bars show the interquartile range, and the black dots indicate the middle 90th percentile of the data. Black line shows a power law model fit to the binned data. No models were fit to the stokes relationships due to the velocity range (> 100 m/yr) which is limited in our analysis.

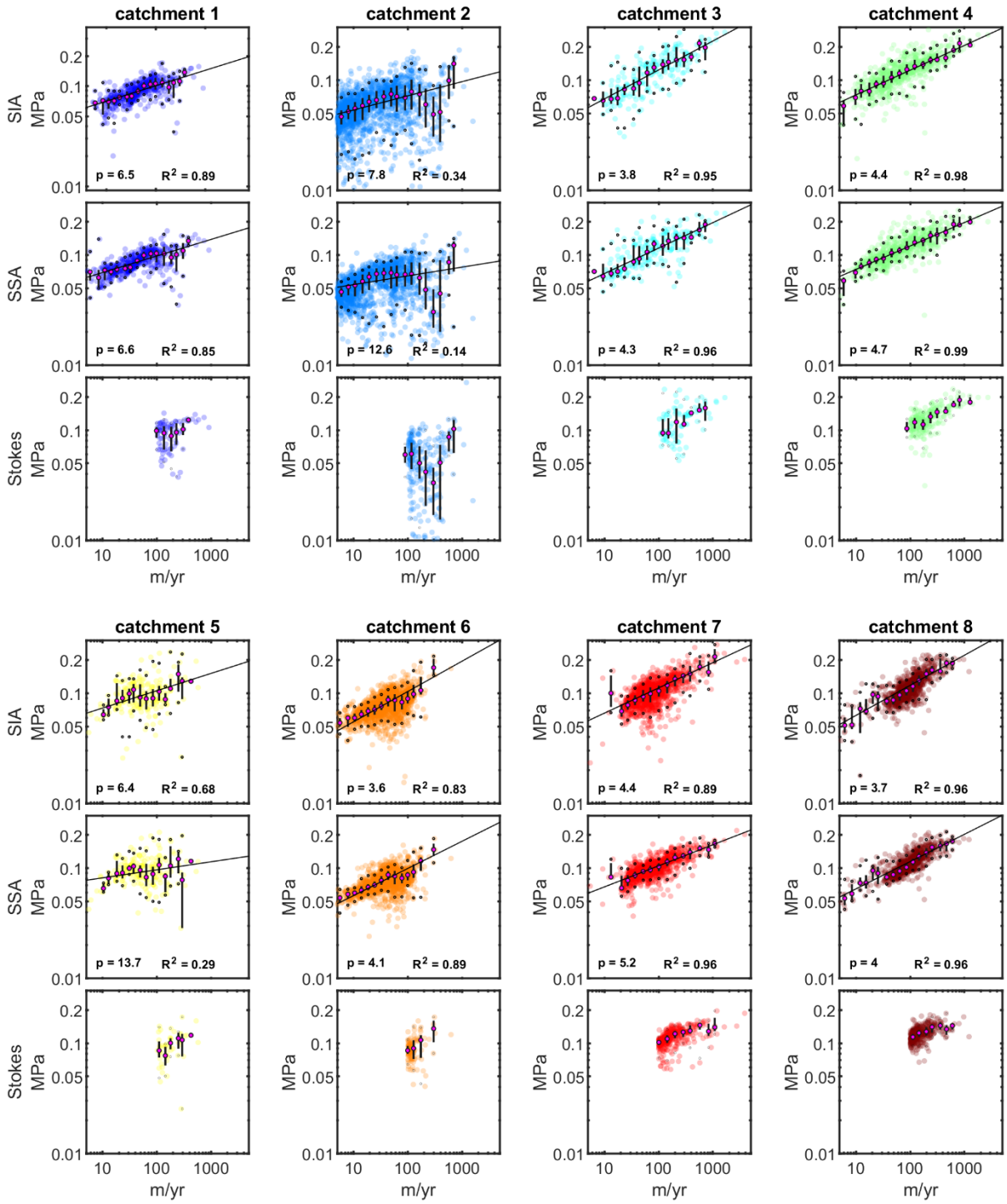

Figure S3 – The velocity – traction relationship for the SIA , SSA, and Full Stokes inversions using 9 km grid cells. Transparency is an indicator of data density, where opaque areas indicate four or more grid cells occupy the same marker area on the plot. Magenta markers show the median traction values for 20 logarithimically spaced velocity bins, the vertical bars show the interquartile range, and the black dots indicate the middle 90th percentile of the data. Black line shows a power law model fit to the binned data. No models were fit to the stokes relationships due to the velocity range (> 100 m/yr) which is limited in our analysis.

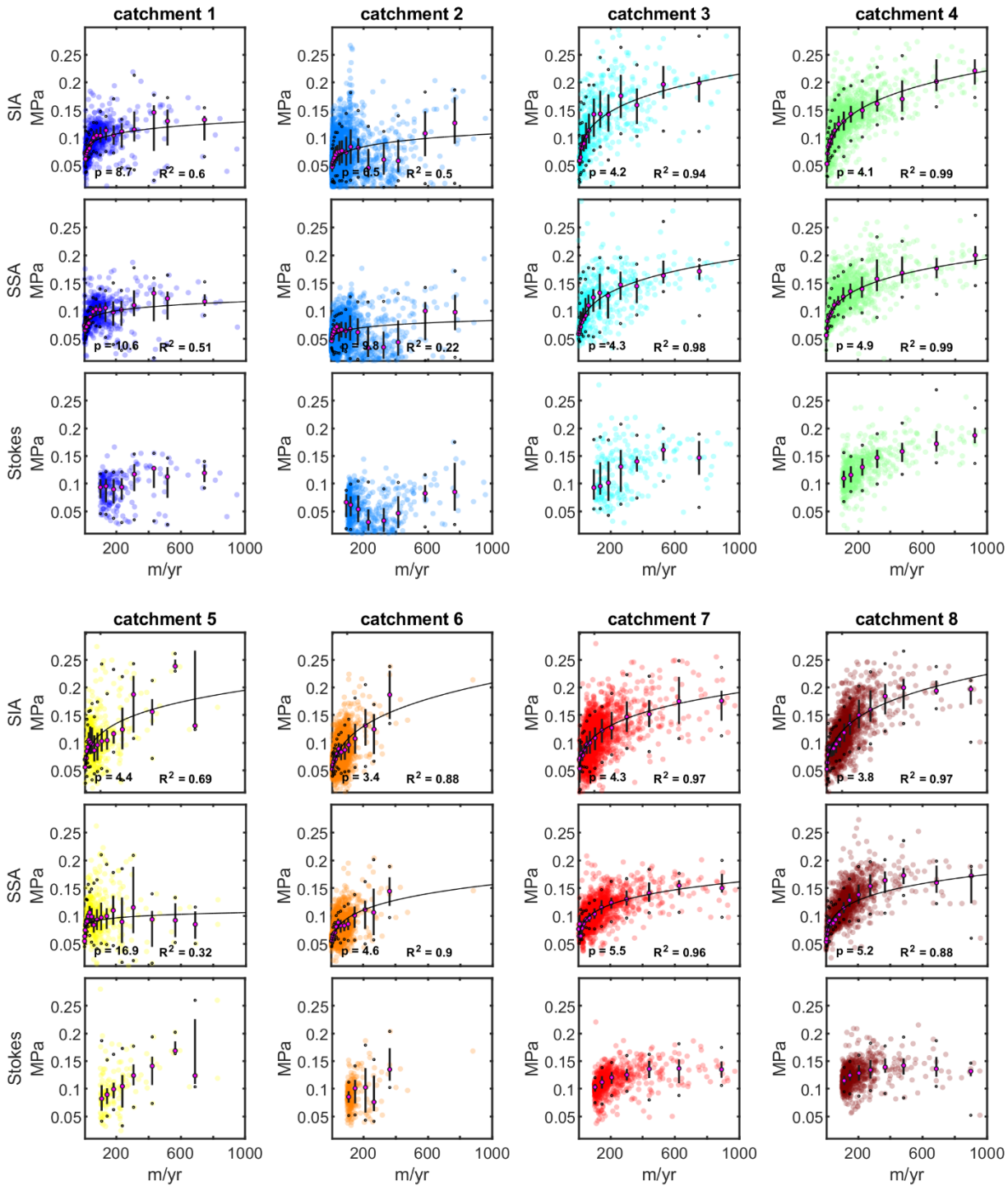

Figure S4 – The velocity – traction relationship for the SIA , SSA, and Full Stokes inversions using 6 km grid cells. Same as *Figure 4*, but plotted on linear scale. Transparency is an indicator of data density, where opaque areas indicate four or more grid cells occupy the same marker area on the plot. Magenta markers show the median traction values for 20 logarithimically spaced velocity bins, the vertical bars show the interquartile range, and the black dots indicate the middle 90th percentile of the data. Black line shows a power law model fit to the binned data. No models were fit to the stokes relationships due to the velocity range (> 100 m/yr) which is limited in our analysis.

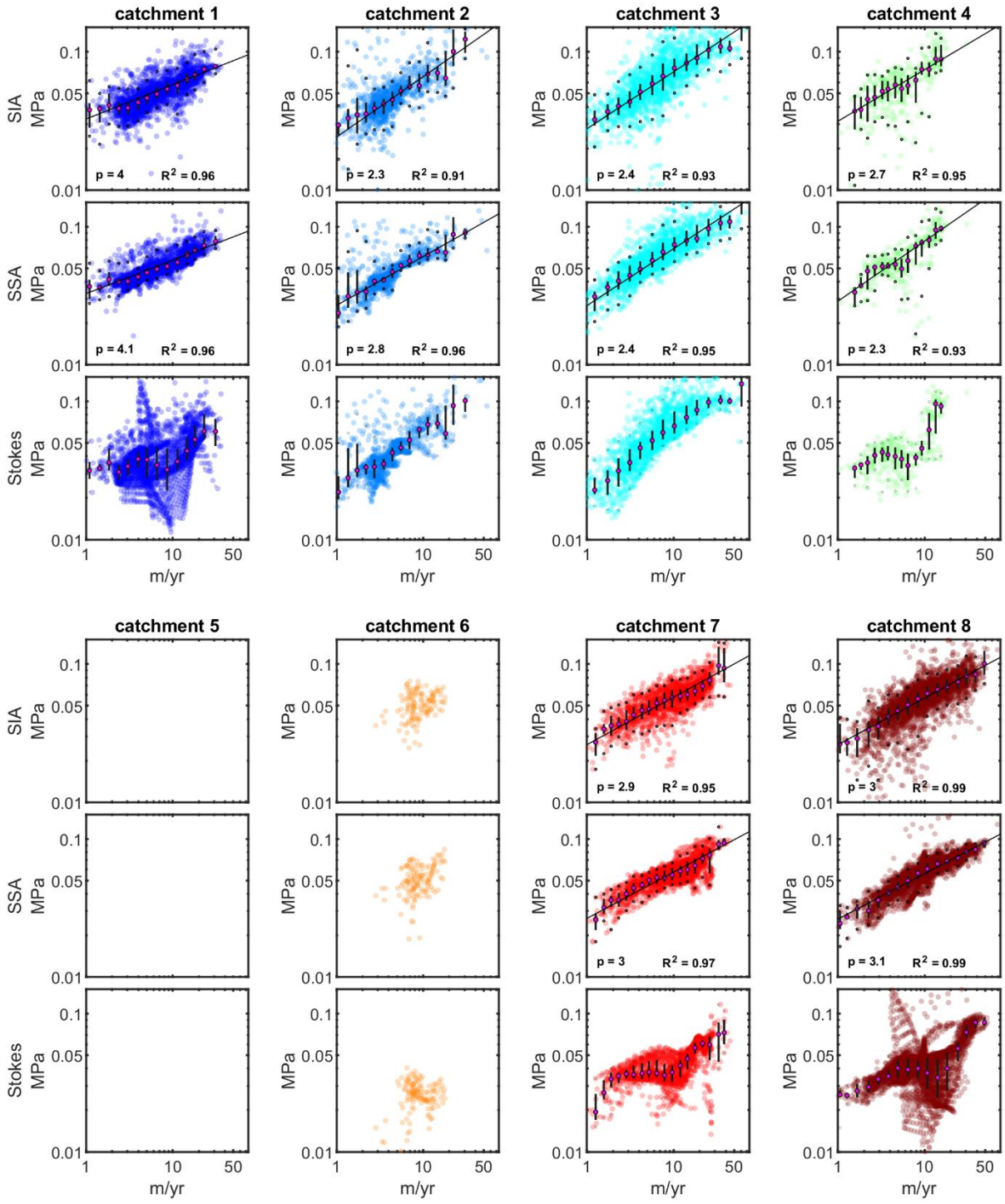

Figure S5 – The velocity – traction relationship for the SIA, SSA, and Full Stokes inversions for the likely-frozen regions of each catchment. Transparency is an indicator of data density, where opaque areas indicate four or more grid cells occupy the same marker area on the plot. Magenta markers show the median traction values for 20 logarithimically spaced velocity bins, the vertical bars show the interquartile range, and the black dots indicate the middle 90th percentile of the data. Black line shows a power law model fit to the binned data. No models were fit to the stokes relationships which have coarse mesh resolution in the inland areas of the ice sheet.

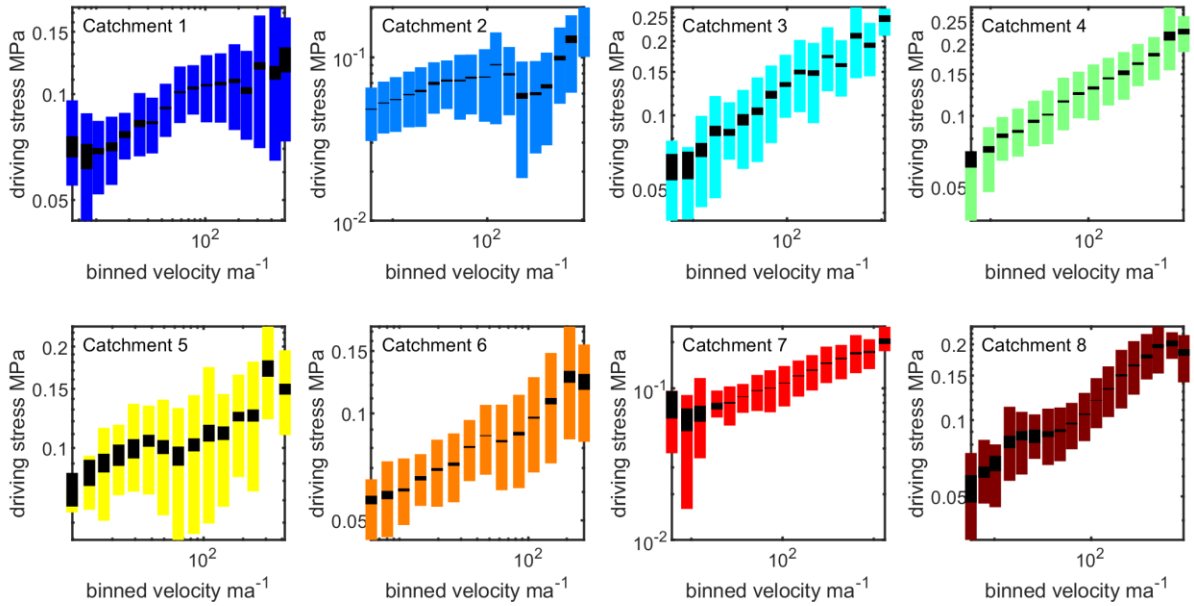

95

Figure S6 – The observed variability (1 σ) from the mean velocity – SIA traction is shown for each velocity bin (colored bars) and catchments. The black bars show the variability estimated for the quantifiable sources of error and uncertainty.

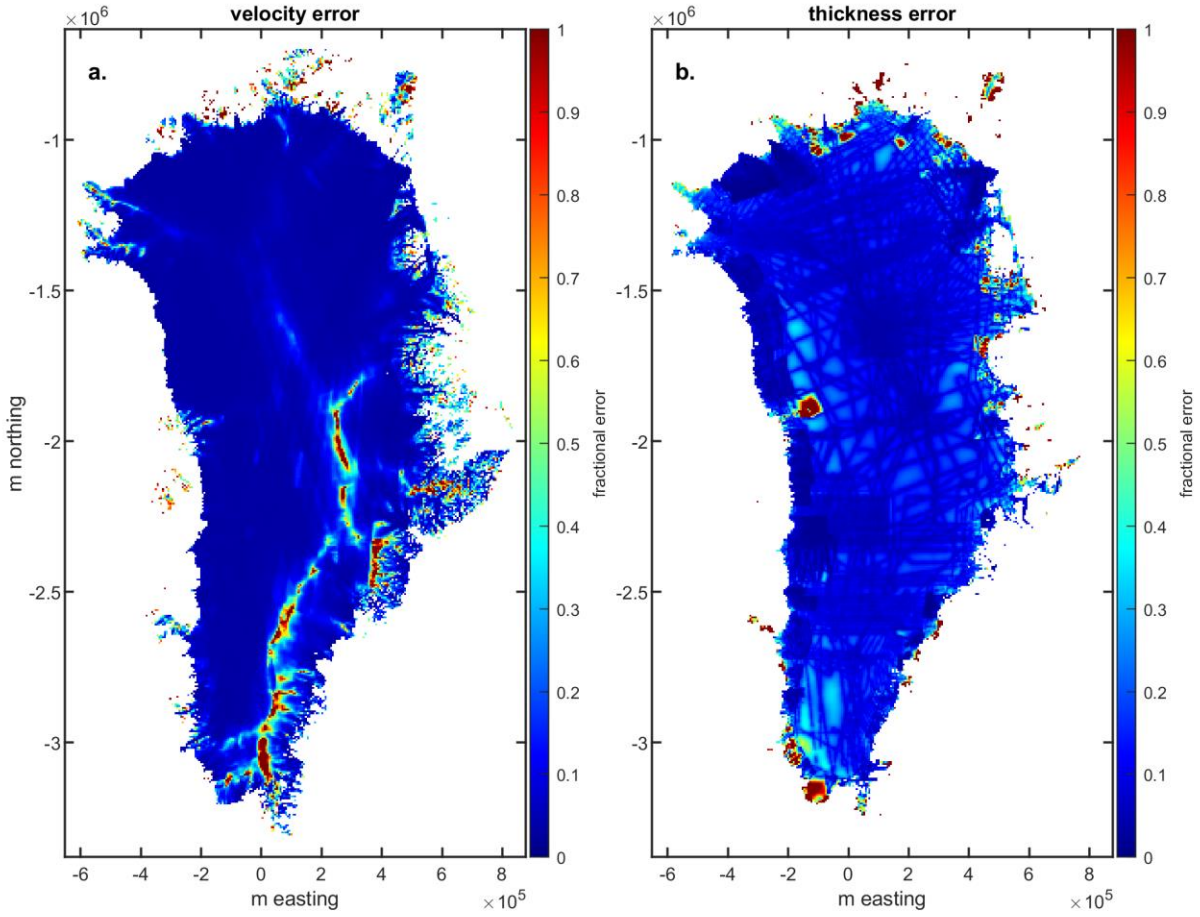

Figure S7 – Fractional error for the velocities (a.) and ice thickness (b.) from the multi-year velocity mosaic (Joughin et al., 2016, 2018) and BedMachine v3 (150 m resolution) (Morlighem, 2018; Morlighem et al., 2017) data sets respectively. Thickness error is the main source of error of uncertainty for estimating the basal traction using the SIA in our analysis.

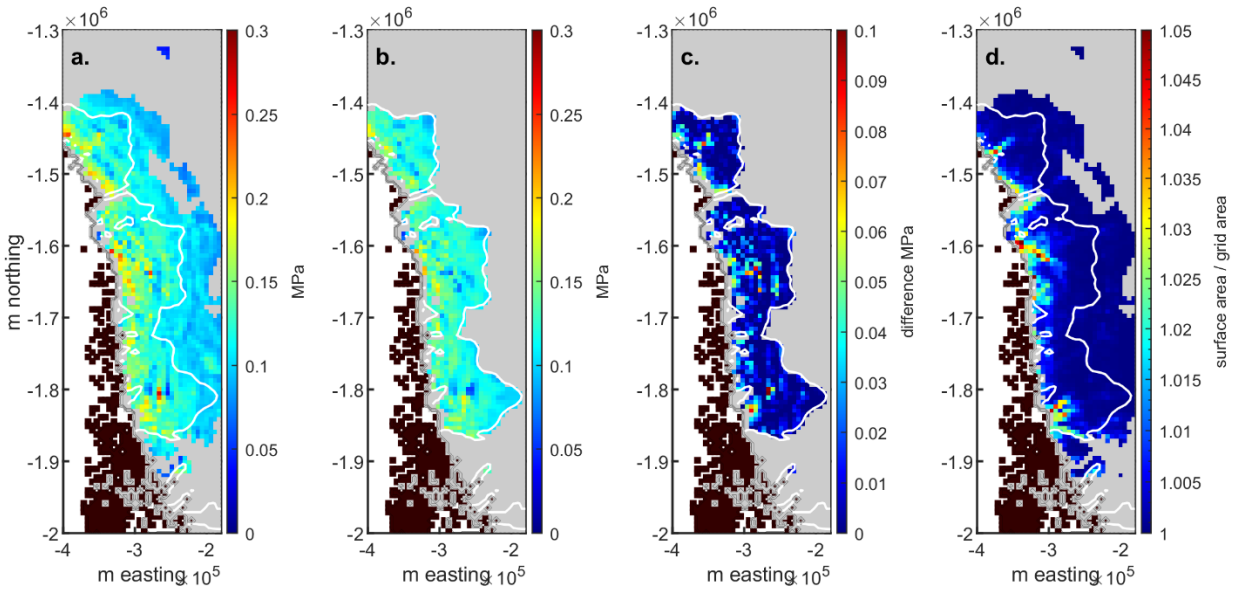

Figure S8 – Panel **a.** and **b.** show the basal traction in catchment 8 for the SSA and FS respectively. Panel **c.** shows the difference between the two traction estimates. Panel **d.** shows the roughness defined as the surface area divided by the grid area of each grid cell. White line shows the 100 m/yr boundary for the FS traction field.

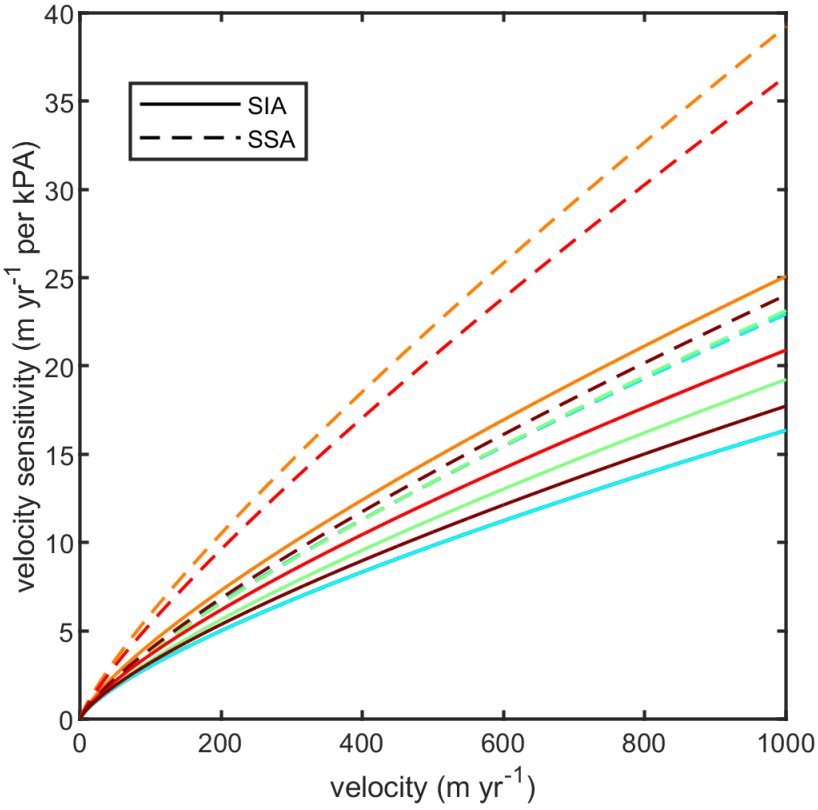

Figure S9 – The velocity sensitivity to traction changes as a function of the velocity for catchments 3, 4, and 6– 8 (3 – blue, 4 – green, 6 – orange, 7 – red, 8 – burgendy) which were characterized as rate strengthening. The velocity sensitivity, which is the rate of velocity change per traction change, is calculated using the parameters (*Table S1*) from the models shown on *Figure 4*.

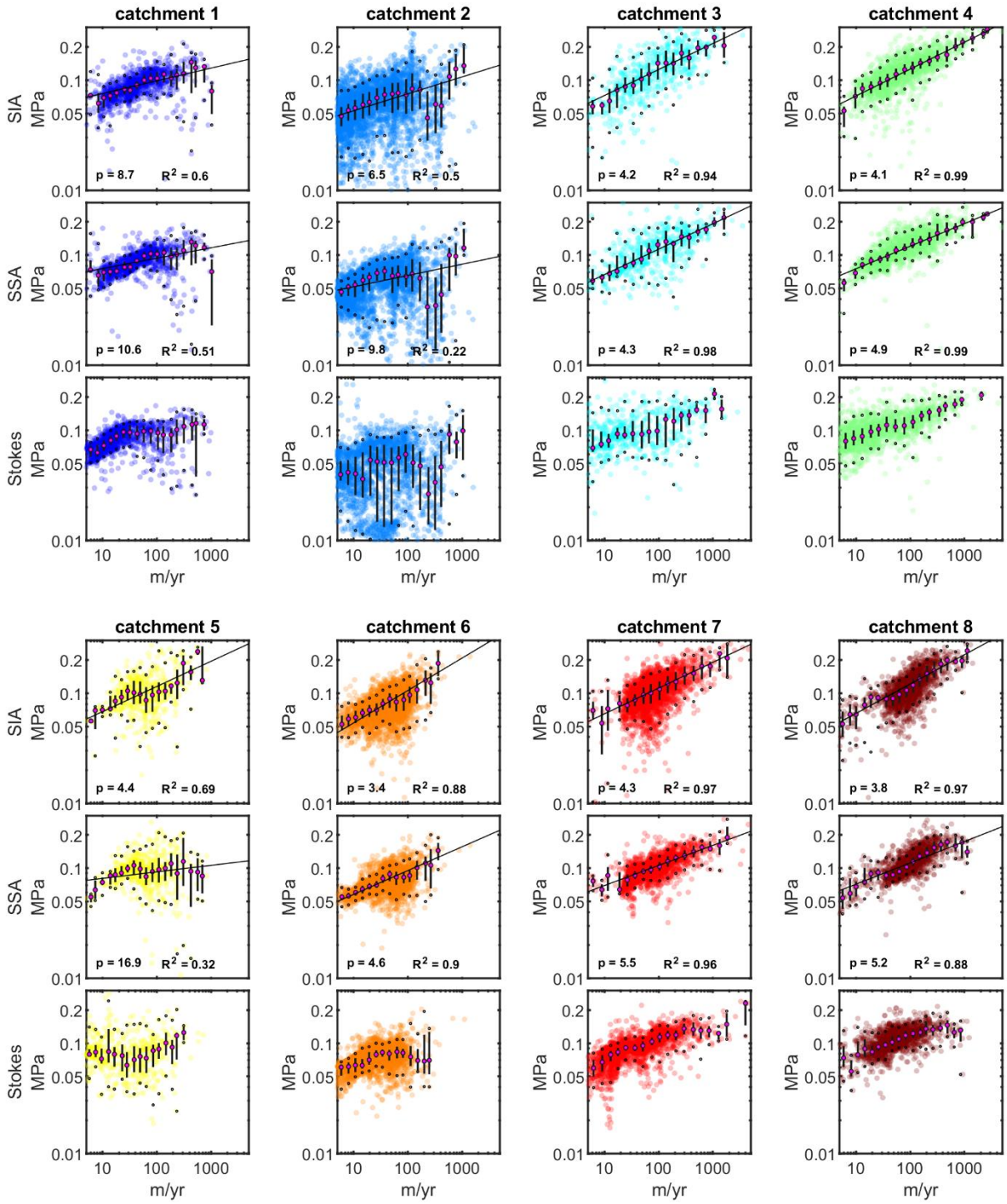

Figure S10 – The velocity – traction relationship for the SIA, SSA, and Full Stokes inversions using 6 km grid cells. This is the same as Figure 4 in the main text, except the FS uses the modelled sliding velocity instead of surface velocity. Transparency is an indicator of data density, where opaque areas indicate four or more grid cells occupy the same marker area on the plot. Magenta markers show the median traction values for 20 logarithimically spaced velocity bins, the vertical bars show the interquartile range, and the black dots indicate the middle 90th percentile of the data. Black line shows a power law model fit to the binned data.

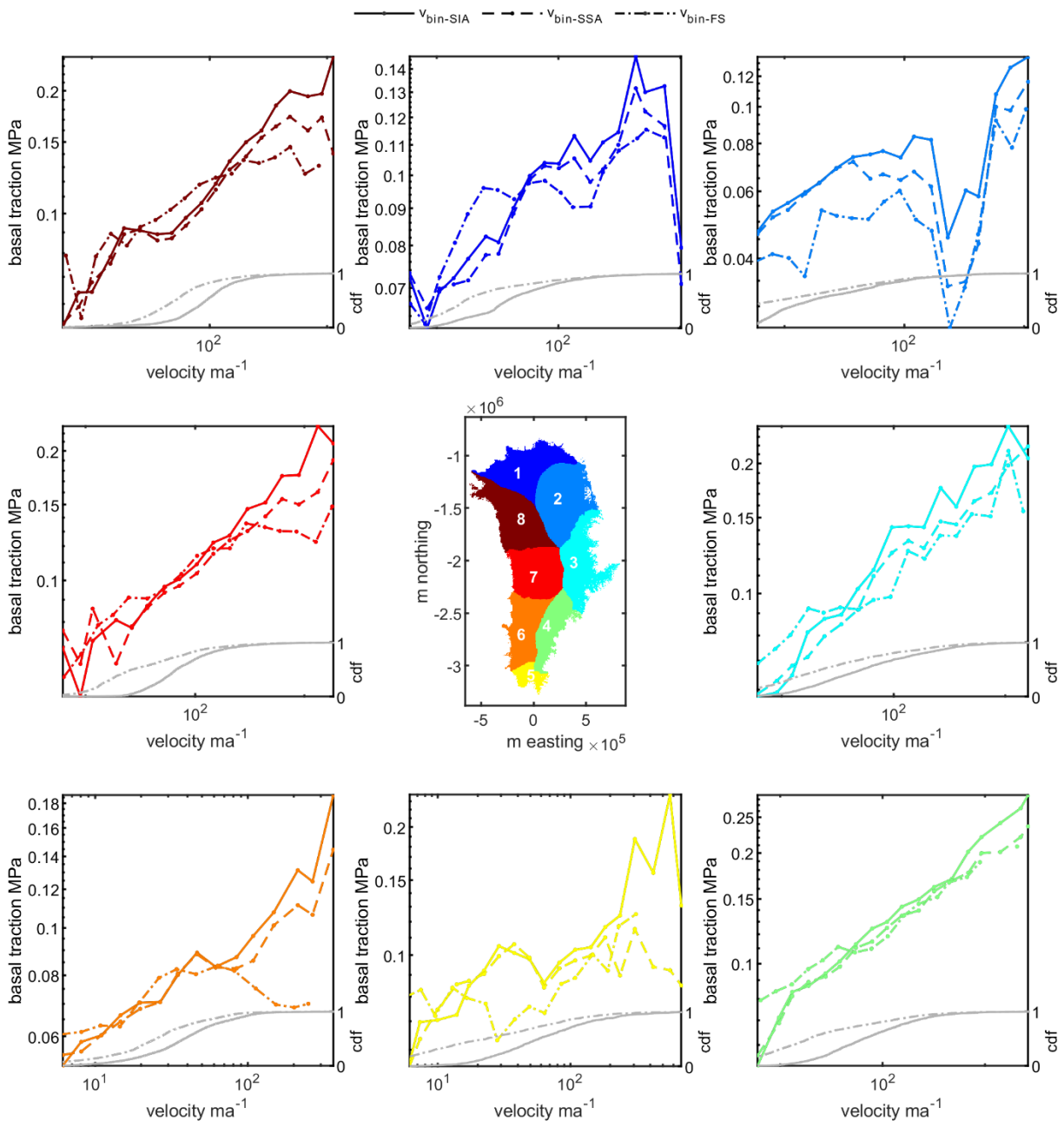

Figure S11 – The relationship between velocity and traction for the SIA (solid line), SSA (dashed line), and FS (dot-dash line) are shown together for each catchment. This is the same as Figure 4 in the main text, except the FS uses the modelled sliding velocity instead of surface velocity. The right axis shows the cumulative distribution function of the data (grey line - SIA SSA, dashed grey line - FS) moving through the velocity range.

Supplementary Tables

Table S1 – Fitting Summary

Catchment	SIA		SSA	
1	R^2 : 0.60 $RMSE$: 0.015 MPa	p : 8.7 [4.8 – 12.5] C_p: 0.058 [0.043 – 0.073]	R^2 : 0.51 $RMSE$: 0.015 MPa	p : 10.6 [5.0 – 16.1] C_p: 0.061 [0.045 – 0.076]
2	R^2 : 0.50 $RMSE$: 0.018 MPa	p : 6.5 [3.1 – 9.9] C_p: 0.037 [0.021 – 0.053]	R^2 : 0.22 $RMSE$: 0.020 MPa	p : 9.8 [0.4 – 19.2] C_p: 0.041 [0.020 – 0.061]
3	R^2 : 0.94 $RMSE$: 0.015 MPa	p : 4.2 [3.6 – 4.9] C_p: 0.042 [0.033 – 0.051]	R^2 : 0.98 $RMSE$: 0.006 MPa	p : 4.3 [4.0 – 4.6] C_p: 0.039 [0.035 – 0.043]
4	R^2 : 0.99 $RMSE$: 0.006 MPa	p : 4.1 [3.9 – 4.3] C_p: 0.041 [0.038 – 0.044]	R^2 : 0.99 $RMSE$: 0.005 MPa	p : 4.9 [4.6 – 5.1] C_p: 0.047 [0.044 – 0.050]
5	R^2 : 0.69 $RMSE$: 0.025 MPa	p : 4.4 [2.8 – 5.9] C_p: 0.040 [0.023 – 0.057]	R^2 : 0.32 $RMSE$: 0.013 MPa	p : 16.9 [3.7 – 30] C_p: 0.071 [0.055 – 0.086]
6	R^2 : 0.88 $RMSE$: 0.013 MPa	p : 3.4 [2.6 – 4.2] C_p: 0.027 [0.019 – 0.036]	R^2 : 0.90 $RMSE$: 0.008 MPa	p : 4.6 [3.7 – 5.6] C_p: 0.035 [0.028 – 0.042]
7	R^2 : 0.97 $RMSE$: 0.009 MPa	p : 4.3 [3.8 – 4.7] C_p: 0.038 [0.032 – 0.044]	R^2 : 0.96 $RMSE$: 0.008 MPa	p : 5.5 [4.8 – 6.1] C_p: 0.046 [0.040 – 0.051]
8	R^2 : 0.97 $RMSE$: 0.010 MPa	p : 3.8 [3.4 – 4.1] C_p: 0.035 [0.030 – 0.041]	R^2 : 0.88 $RMSE$: 0.014 MPa	p : 5.2 [4.1 – 6.2] C_p: 0.046 [0.036 – 0.056]

Notes: Bracketed values show 95% confidence interval for each model parameter.

Table S2 – Stress conditions at field locations where till was identified

Study	Methods Used	Site Characteristics	Driving Stress (self reported)	Driving Stress (estimated 10 H)
Dow 2013	Seismic AVA	Land terminating, low elevation, inland from margin of Russel Glacier	none	0.1 MPa
Booth 2012, Kulessa 2017	Seismic AVA	Land terminating, Russel sector, high elevation, adjacent to supraglacial lake	none	0.08 MPa
Doyle 2018, Hofstede, 2018	Seismic AVA, Borehole Observation	Marine terminating, inland from Store Glacier terminus	0.22 MPa	0.21 MPa
Walter 2014, Ryser 2014a	Seismic AVA, Borehole Observation	Land terminating, north of Jakobshavn, topographic trough (Site Name: Fox)	0.17 MPa	0.14 MPa
Ryser 2014a	Borehole Observation	Land terminating, north of Jakobshavn, topographic trough, inland from Fox (Site Name: Gull)	0.13 MPa	0.11 MPa

Notes: Self-reported driving stress values were either directly reported within the manuscript or calculated from the reported ice thickness and surface slope assuming an ice density of 900 kg/m^3. Estimated driving stress values were calculated identically to the SIA traction in our manuscript with the grid cell centered on the site location and cell dimensions equivalent to 10 ice thicknesses.

References

Alley, R. B.: Flow-law hypotheses for ice-sheet modeling, Journal of Glaciology, 38(129), 245–256, 1992.

Andrews, L. C., Catania, G. A., Hoffman, M. J., Gulley, J. D., Lüthi, M. P., Ryser, C., Hawley, R. L. and Neumann, T. A.: Direct observations of evolving subglacial drainage beneath the Greenland Ice Sheet, Nature, 514(7520), 80, 2014.

Andrews, L. C., Hoffman, M. J., Neumann, T. A., Catania, G. A., Lüthi, M. P., Hawley, R. L., Schild, K. M., Ryser, C. and Morriss, B. F.: Seasonal evolution of the subglacial hydrologic system modified by supraglacial lake drainage in western Greenland, Journal of Geophysical Research: Earth Surface, 123(6), 1479–1496, 2018.

Bartholomew, I., Nienow, P., Mair, D., Hubbard, A., King, M. A. and Sole, A.: Seasonal evolution of subglacial drainage and acceleration in a Greenland outlet glacier, Nature Geoscience, 3(6), 408–411, 2010.

Bartholomew, I., Nienow, P., Sole, A., Mair, D., Cowton, T., Palmer, S. and Wadham, J.: Supraglacial forcing of subglacial drainage in the ablation zone of the Greenland ice sheet, Geophysical Research Letters, 38(8), 2011.

Bartholomew, I., Nienow, P., Sole, A., Mair, D., Cowton, T. and King, M. A.: Short-term variability in Greenland Ice Sheet motion forced by time-varying meltwater drainage: Implications for the relationship between subglacial drainage system behavior and ice velocity, Journal of Geophysical Research: Earth Surface, 117(F3), 2012.

Bons, P. D., Kleiner, T., Llorens, M., Prior, D. J., Sachau, T., Weikusat, I. and Jansen, D.: Greenland Ice Sheet: Higher nonlinearity of ice flow significantly reduces estimated basal motion, Geophysical Research Letters, 45(13), 6542–6548, 2018.

Cowton, T., Nienow, P., Sole, A., Bartholomew, I. and Mair, D.: Variability in ice motion at a land-terminating Greenlandic outlet glacier: the role of channelized and distributed drainage systems, Journal of Glaciology, 62(233), 451–466, 2016.

Cuffey, K. M. and Paterson, W. S. B.: The Physics of Glaciers, Academic Press., 2010.

Dahl-Jensen, D. and Gundestrup, N.: Constitutive properties of ice at Dye 3, Greenland, International Association of Hydrological Sciences Publication, 170, 31–43, 1987.

Gagliardini, O., Zwinger, T., Gillet-Chaulet, F., Durand, G., Favier, L., De Fleurian, B., Greve, R., Malinen, M., Martín, C. and Råback, P.: Capabilities and performance of Elmer/Ice, a new-generation ice sheet model, Geoscientific Model Development, 6(4), 1299–1318, 2013.

Gillet-Chaulet, F., Hindmarsh, R. C., Corr, H. F., King, E. C. and Jenkins, A.: In-situquantification of ice rheology and direct measurement of the Raymond Effect at Summit, Greenland using a phase-sensitive radar, Geophysical Research Letters, 38(24), 2011.

Hoffman, M., Catania, G. A., Neumann, T., Andrews, L. and Rumrill, J.: Links between acceleration, melting, and supraglacial lake drainage of the western Greenland Ice Sheet, Journal of Geophysical Research: Earth Surface, 116(F4), 2011.

Joughin, I., Smith, B., Howat, I. and Scambos, T.: MEaSUREs Multi-year Greenland Ice Sheet Velocity Mosaic, Version 1, Boulder, Colorado USA. NASA National Snow and Ice Data Center Distributed Active Archive Center, 2016.

Joughin, I., Smith, B. E. and Howat, I. M.: A complete map of Greenland ice velocity derived from satellite data collected over 20 years, Journal of Glaciology, 64(243), 1–11, 2018.

Kulessa, B., Hubbard, A. L., Booth, A. D., Bougamont, M., Dow, C. F., Doyle, S. H., Christoffersen, P., Lindbäck, K., Pettersson, R., Fitzpatrick, A. A. W. and Jones, G. A.: Seismic evidence for complex sedimentary control of Greenland Ice Sheet flow, Science Advances, 3(8), e1603071, 2017.

Lüthi, M., Funk, M., Iken, A., Gogineni, S. and Truffer, M.: Mechanisms of fast flow in Jakobshavn Isbræ, West Greenland: Part III. Measurements of ice deformation, temperature and cross-borehole conductivity in boreholes to the bedrock, Journal of Glaciology, 48(162), 369–385, 2002.

Montagnat, M. and Duval, P.: The viscoplastic behaviour of ice in polar ice sheets: experimental results and modelling, Comptes Rendus Physique, 5(7), 699–708, 2004.

Morlighem, M.: IceBridge BedMachine Greenland, Version 3, Boulder, Colorado USA. NASA National Snow and Ice Data Center Distributed Active Archive Center, doi:https://doi.org/10.5067/2CIX82HUV88Y, 2018.

Morlighem, M., Williams, C. N., Rignot, E., An, L., Arndt, J. E., Bamber, J. L., Catania, G., Chauché, N., Dowdeswell, J. A. and Dorschel, B.: BedMachine v3: Complete bed topography and ocean bathymetry mapping of Greenland from multibeam echo sounding combined with mass conservation, Geophysical Research Letters, 44(21), 11–051, 2017.

Russell-Head, D. and Budd, W.: Ice-sheet flow properties derived from bore-hole shear measurements combined with ice-core studies, Journal of Glaciology, 24(90), 117–130, 1979.

Ryser, C., Lüthi, M. P., Andrews, L. C., Catania, G. A., Funk, M., Hawley, R., Hoffman, M. and Neumann, T. A.: Caterpillar-like ice motion in the ablation zone of the Greenland ice sheet, Journal of Geophysical Research: Earth Surface, 119(10), 2258–2271, 2014a.

Ryser, C., Lüthi, M. P., Andrews, L. C., Hoffman, M. J., Catania, G. A. and Hawley, R. L.: Sustained high basal motion of the Greenland ice sheet revealed by borehole deformation, Journal of Glaciology, 2014b.

Sole, A., Nienow, P., Bartholomew, I., Mair, D., Cowton, T., Tedstone, A. and King, M. A.: Winter motion mediates dynamic response of the Greenland Ice Sheet to warmer summers, Geophysical Research Letters, 40(15), 3940–3944, 2013.

Stevens, L. A., Behn, M. D., McGuire, J. J., Das, S. B., Joughin, I., Herring, T., Shean, D. E. and King, M. A.: Greenland supraglacial lake drainages triggered by hydrologically induced basal slip, Nature, 522(7554), 73–76, 2015.